Nuclear Inst, and Methods in Physics Research B 424 (2018) 1–9

Contents lists available at ScienceDirect

Nuclear Inst. and Methods in Physics Research B

journal homepage: www.elsevier.com/locate/nimb

Secondary ion formation during electronic and nuclear sputtering of germanium

L. Breuer[a], P. Ernst[a], M. Herder[a], F. Meinerzhagen[a], M. Bender[b], D. Severin[b], A. Wucher[a,*]

[a] Fakultät für Physik, Universität Duisburg-Essen, 47048 Duisburg, Germany
[b] GSI Helmholtz Zentrum für Schwerionenforschung, 64291 Darmstadt, Germany

ARTICLE INFO

Keywords:
Swift heavy ions
Electronic sputtering
Ionization probability
Post-ionization

ABSTRACT

Using a time-of-flight mass spectrometer attached to the UNILAC beamline located at the GSI Helmholtz Centre for Heavy Ion Research, we investigate the formation of secondary ions sputtered from a germanium surface under irradiation by swift heavy ions (SHI) such as 5 MeV/u Au by simultaneously recording the mass spectra of the ejected secondary ions and their neutral counterparts. In these experiments, the sputtered neutral material is post-ionized via single photon absorption from a pulsed, intensive VUV laser. After post-ionization, the instrument cannot distinguish between secondary ions and post-ionized neutrals, so that both signals can be directly compared in order to investigate the ionization probability of different sputtered species. In order to facilitate an in-situ comparison with typical nuclear sputtering conditions, the system is also equipped with a conventional rare gas ion source delivering a 5 keV argon ion beam. For a dynamically sputter cleaned surface, it is found that the ionization probability of Ge atoms and Ge_n clusters ejected under electronic sputtering conditions is by more than an order of magnitude higher than that measured for keV sputtered particles. In addition, the mass spectra obtained under SHI irradiation show prominent signals of Ge_nO_m clusters, which are predominantly detected as positive or negative secondary ions. From the *m*-distribution for a given Ge nuclearity *n*, one can deduce that the sputtered material must originate from a germanium oxide matrix with approximate GeO stoichiometry, probably due to residual native oxide patches even at the dynamically cleaned surface. The results clearly demonstrate a fundamental difference between the ejection and ionization mechanisms in both cases, which is interpreted in terms of corresponding model calculations.

1. Introduction

The formation of secondary ions during ion sputtering of solid surfaces represents the physical basis of secondary ion mass spectrometry (SIMS). A key quantity in such experiments is the ionization probability of a sputtered particle, and significant effort has therefore been devoted to investigate this quantity under so-called *nuclear sputtering* conditions, where the surface is bombarded with keV projectile ions and the primary energy transfer is dominated by nuclear stopping. Much less is known about secondary ion formation in the *electronic sputtering* regime, where the solid is irradiated with swift heavy ions (SHI) and the primary energy transfer occurs via electronic stopping of the projectile. While the ionized particles ejected from the surface under these conditions have been characterized for a few target materials (mainly ionic crystals such as LiF [1–23]), including measurements of secondary ion yields as well as the emission velocity and angle distributions of sputtered atomic and cluster ions [12,14,15,18,20,21], to date practically no such information exists about the sputtered material which is emitted in the neutral charge state. Using collector techniques, total sputter yields as well as angular distributions of the sputtered material have been measured for some ion-target combinations (for a review see [24]), which – provided the instrumental transmission and detection efficiency for the secondary ions is known – in principle allow to estimate the total ion fraction of the sputtered material. A fundamental open question, however, regards the ion fraction of specific components in the sputtered flux. In that context, it is useful to define the ionization probability of a sputtered species X as

$$\alpha_X^{+,-} = \frac{Y_X^{+,-}}{Y_X}, \tag{1}$$

where X can stand for an emitted single atom, molecule or cluster, respectively. The quantity $Y_X^{+,-}$ denotes the secondary ion yield, i.e., the average number of secondary ions $X^{+,-}$ which is emitted per projectile impact, while Y_X represents the respective partial sputter yield of all emitted particles X regardless of their charge state. It should be stressed that this definition of $\alpha_X^{+,-}$ does not necessarily imply the emission and

* Corresponding author.
E-mail address: andreas.wucher@uni-due.de (A. Wucher).

https://doi.org/10.1016/j.nimb.2018.03.019
Received 14 October 2017; Received in revised form 2 February 2018; Accepted 13 March 2018
Available online 28 March 2018
0168-583X/

ionization processes to be decoupled from each other. While this may in some cases be true, e.g. for single atoms emitted from a clean metallic surface under nuclear sputtering conditions, one could imagine a strong coupling between the ejection and ionization mechanisms in other cases, for instance via a charge related emission process such as Coulomb explosion. Particularly for molecular emission, the fragmentation or survival of a sputtered molecule may also be closely coupled to its charge state, so that the factorization according to Eq. (1) may represent an oversimplification. Moreover, both the emission velocity and angle distributions of secondary ions may in principle differ from those of the respective neutral particles, thereby defining a velocity or trajectory dependent ionization probability of a sputtered particle.

The goal to obtain quantitative information regarding the ionization probability of sputtered particles ultimately requires the mass resolved detection of emitted neutral species in addition to the corresponding secondary ions under otherwise identical experimental conditions. This is a difficult task, since neutral particles must be post-ionized in order to render them accessible for mass spectrometric analysis. Several post-ionization schemes have been employed, including electron impact ionization (using either an electron beam [25] or the electron component of a low pressure plasma [26]), surface ionization (involving scattering of the particles at a heated surface) or photoionization (using resonant or non resonant multiphoton or strong field ionization [27]). Among these, single photon ionization (SPI) using an intense VUV laser has been demonstrated as a promising tool for efficient post-ionization of atoms and molecules, provided the photon energy is above the ionization potential of the investigated species [28–33]. If combined with time-of-flight (ToF) mass spectrometry, it was shown that this technique allows the detection of secondary ions and their neutral counterparts under otherwise identical experimental conditions regarding the detection probability as well as the sampled emission angle and velocity window [27]. Moreover, it is often possible to drive the photoionization process into saturation, thereby gaining quantitative information about the post-ionization efficiency which is essential for a determination of absolute ionization probability values.

We have frequently employed this technique in the past in order to measure the ionization probability of particles emitted under nuclear sputtering conditions [30,34–44]. For elemental targets, it is found that the ionization probability strongly depends on a possible surface contamination, an effect which is commonly described as the SIMS matrix effect. For thoroughly sputter cleaned surfaces, one usually finds relatively small values $< 10^{-3}$ for sputtered single atoms [45], which increase for clusters with increasing cluster size [30,34,37,46–48]. Oxidized surfaces, on the other hand, yield ionization probabilities which may be enhanced by orders of magnitude [49–51]. Only recently, a ToF spectrometer equipped with a VUV post-ionization laser was added to a high energy ion beam line [52], thereby allowing to adopt the technique to particles emitted under electronic sputtering conditions as well [53]. In this work, we present data collected on atoms and clusters ejected from a dynamically sputter cleaned germanium surface and compare the results obtained under SHI impact with those measured in-situ under low energy rare gas ion bombardment.

2. Experimental

The experiments were performed using a home-built reflectron time-of-flight (ToF) mass spectrometer installed at the M1 beam line of the UNILAC accelerator facility at the Helmholtz centre for heavy ion research (GSI) in Darmstadt, Germany. The system has been described in detail elsewhere [52], and therefore only a brief description of the features relevant for this work will be given here. The ToF spectrometer is mounted under 45° with respect to the UNILAC ion beam, and the sample is positioned in such a way that the sputtered particles are collected along the surface normal. For reference and alignment purposes, the system also includes a 5 keV Argon ion beam which impinges under the same polar angle (45°) with respect to the surface normal as the SHI projectiles. Projectile ions used in these experiments were ^{197}Au ions of a selected charge state (26 +) delivered by the accelerator with a specific energy of 4.8 MeV/u. We note that these conditions do not coincide with the equilibrium charge state of the gold ions (which is reached once the projectile penetrates a distance of typically several 10 nm into the solid), and therefore the energy deposition from electronic stopping of the projectile will vary as a function of penetration depth [54]. For the sputtering process investigated here, however, this variation is practically irrelevant since the mean emission depth of sputtered particles is only of the order of several nm. The UNILAC beam was shaped to a spot profile of typically about 6 mm diameter using a fluorescent target in place of the sample. The spot profile of the keV-beam was also examined by the fluorescent target and set to a diameter of about 2 mm FWHM.

Secondary ions released from the surface were swept into the ToF spectrometer using a pulsed extraction field, with the switching time marking the flight time zero for the detected ions. The reflector voltage (1450 V) was tuned slightly below the target potential (1600 V) in order to ensure that only ions originating from a minimum height of about 1 mm above the sample surface could be reflected and detected. In connection with the flight time refocusing properties of the ToF spectrometer, this setting determines a sensitive volume of about 1 mm diameter located at about 1 mm above the surface and centered around the ion optical axis of the spectrometer, from which ions could be extracted and contribute to the detected sharp flight time peaks [27].

Secondary neutral particles emerging from the bombarded surface were post-ionized using a pulsed F_2-laser operated at a VUV wavelength of 157 nm. The corresponding photon energy ensured that neutral atoms and molecules possessing ionization potentials up to 7.9 eV can be efficiently post-ionized via non resonant single photon absorption. The laser beam was directed parallel to the sample surface at a distance matching the location of the ToF sensitive volume. The beam was focused to a spot diameter of about 0.5 mm using a 250 mm focal length CaF_2 lens, which at the same time acted as the entrance window to the ultrahigh vacuum chamber housing the experiment. The laser delivered output pulses of about 4–7 ns duration and up to about 1.6 mJ pulse energy, which was monitored using its internal energy monitor and calibrated using a GenTech power meter. Due to geometrical restrictions, the laser beam had to be guided through an evacuated beam line of about 2 m length and then coupled into the vacuum system via a ~120° deflecting mirror, both leading to a significant intensity loss before being introduced into the experiment chamber. The intensity of the laser pulse actually entering the vacuum chamber was therefore monitored again with a fast in-vacuum photoelectric detector located behind the sample, the signal of which was also used in order to control the timing of the pulse.

During most of the experiments, the laser pulse was fired simultaneously with the ion extraction pulse. This way, the instrument cannot distinguish between intrinsic secondary ions and post-ionized neutral particles of the same species, thereby detecting both entities under otherwise the same experimental conditions regarding instrument transmission and detection efficiency. In order to distinguish between secondary ions and post-ionized neutrals, spectra were therefore taken with (SNMS) and without (SIMS) firing the laser beam, and the data corresponding to the secondary neutral particles alone were derived by subtracting both spectra. In the following, the spectra taken under irradiation with swift heavy ions during an UNILAC pulse will be referred to as “MeV-SNMS” and “MeV-SIMS”, respectively.

Inbetween subsequent UNILAC pulses, additional spectra were taken either with the keV argon ion beam bombarding the surface (“keV-SNMS/SIMS”) or without any ion bombardment at all. While the first deliver reference spectra which allow a direct comparison between electronic and nuclear sputtering processes, the latter are needed to ensure that the measured signals are actually related to the ion bombardment. In particular, the data taken with the laser beam alone reveals important information about the background signal arising from

laser photoionization of residual gas components, while the blank spectrum measured without ion or laser beam basically shows the detector baseline. All six spectra (MeV-SNMS, MeV-SIMS, keV-SNMS, keV-SIMS, residual gas and blank) were obtained in a highly interleaved manner during a single UNILAC pulse cycle and summed over a desired number of such cycles in order to achieve the targeted counting statistics.

Secondary ions and post-ionized neutral particles were detected using a Chevron stack of two microchannel plates (MCP) equipped with a grounded entrance grid. A post-acceleration voltage of 4 kV was applied between the grid and the MCP front, leading to a total ion impact energy of 5.6 keV onto the detector. The MCP output current was measured on a collector plate and digitized using a fast transient digitizer board (Signatec PX 1500). The 8 bit digitizer delivers byte values between 0 and 255, which will in the following be referred to as “cts”. Note that the unit of 1 ct defined this way does *not* correspond to the registration of one ion, but rather symbolizes a detected MCP output signal of several mV height, which depends on the MCP gain voltage setting. In order to determine the actual number of detected ions of a particular mass, the corresponding flight time peak must be integrated, and the resulting peak integral must be divided by the average peak integral induced by a single ion impact of the same mass. In many cases, the data were summed over many acquired spectra (“reps”). To allow an easy comparison, the measured signal will in the following be normalized to the number of reps and displayed in units of “cts/rep”.

The ion fluence applied during a single UNILAC pulse varied depending on the UNILAC pulse current and duration (with the latter being set by the accelerator facility) between 10^7 and 10^8 ions/cm^2. Depending on the number of pulse cycles used to acquire the data, the SHI fluence applied during acquisition of one spectrum therefore varied between approximately 10^8 and 10^{11} ions/cm^2. In order to examine the influence of the applied total fluence, pseudo depth profiles were usually measured where spectral data was taken repetitiously without applying additional ion bombardment inbetween. The investigated sample was sputter cleaned prior to the data acquisition using dc bombardment with the keV argon ion beam to a total fluence of the order of 10^{16} ions/cm^2. In order to ensure a defined surface state even during prolonged data acquisition sequences, corresponding to the utmost cleanliness of the surface reachable in our system, the Ar^+ ion beam was interleaved with the data acquisition, leaving it on dc operation during the time period between subsequent data analysis cycles and only temporarily pulsing it off during the UNILAC pulses and the data acquisition gates for blank spectra, respectively. Under these conditions, a dynamical equilibrium between sputter removal and readsorption of residual gas particles is established, with the residual surface contamination being determined by the Ar^+ current density and the residual gas pressure in the vacuum system. Since the experiments were performed under UHV conditions with a base pressure $< 10^{-8}$ mbar, the applied ion current density of $\sim 6 \times 10^{13}$ ions/cm^{2}s, in connection with a realistic sputter yield of ~ 10 atoms/ion and a maximum sticking probability of 1, leads to a maximum possible residual surface contamination of the order of 1 at.%.

Germanium samples were cut from an undoped Ge wafer with an approximately (1 1 1)-oriented surface. However, the crystalline structure of the sample is irrelevant in these experiments since the prebombardment by 5-keV Ar^+ ions leads to complete amorphization of the sample to a depth of several nanometers. The sample was sonicated in isopropanol for a few minutes before mounting on the sample holder using either copper tape or clamping with a Mo mask.

3. Results and discussion

In this work, the ionization probability $\alpha_X^{+,-}$ of a sputtered particle X is investigated by comparison of mass spectrometric signals measured for singly positively or negatively charged secondary ions X^+ or X^- with those measured for their respective neutral counterparts X^0. For the experimental setup used here, these signals can be formally described by

$$S(X^{+,-}) = I_p \cdot Y_X \cdot \eta \cdot \alpha_X^{+,-} \quad \text{and} \quad S(X^0) = I_p \cdot Y_X \cdot \eta \cdot (1-\alpha_X^{+}-\alpha_X^{-}) \cdot \alpha_X^0 \tag{2}$$

where I_p denotes the projectile current, Y_X is the partial sputter yield of species X (regardless of its charge state) and α_X^0 stands for the post-ionization efficiency of the sputtered neutrals. The detection efficiency η describes the fraction of emitted species (secondary ions or post-ionized neutrals) which is effectively sampled by the mass spectrometer. It is determined by the accepted emission velocity and angle window of the ToF spectrometer in combination with the respective emission distributions of the sputtered particles and may therefore in principle be different depending on the detected species and charge state. In that context, it is important to note that our experiment is sensitive to the number density of sputtered particles within the sensitive volume rather than their flux. Particularly if the secondary ions and neutrals are emitted with different velocity distributions, this will lead to a correction factor determined by the average inverse emission velocity

$$\langle v^{-1} \rangle = \int_0^\infty v^{-1} f(v) dv \tag{3}$$

For the specific case of In atoms sputtered from a clean indium surface under 5-keV Ar^+ ion bombardment, the emission velocity distribution $f(v)$ has been measured for In^+ and In^0 secondary ions and neutrals, respectively, revealing a difference by about a factor two between the average inverse emission velocities of both species. Since we are interested in the order of magnitude rather than the exact value of the ionization probability here, we therefore neglect this difference throughout the remainder of this paper.

3.1. Mass spectra

Mass spectra of post-ionized neutral particles and secondary ions detected under 4.8 MeV/u Au^{26+} and 5 keV Ar^+ irradiation of a dynamically sputter cleaned germanium sample are shown in Fig. 1.

It is seen that the spectrum of post-ionized neutral particles emitted under keV ion bombardment (right hand panel of Fig. 1) consists mainly of sputtered neutral Ge atoms and Ge_n clusters, which are detectable here up to $n = 7$, with very small signals of GeO(H) and Ge_2O molecules. The positive secondary ion spectrum observed under these conditions is dominated by the usual Na^+ and K^+ alkali contamination peaks (not shown in Fig. 1), but also shows a prominent signal for Ge^+ ions and the series of Ge_n^+ cluster ions. In addition, the spectrum contains sizeable fractions of $Ge_nO_m^+$ or $Ge_nO_mH^+$ cluster ions even though the surface is sputter cleaned, a finding which is quite common in positive secondary ion mass spectrometry of elemental surfaces since oxygen is known to significantly enhance the positive ionization probability [50]. The negative secondary ion spectrum is dominated by an O^- impurity peak (not shown in Fig. 1) and otherwise shows prominent signals for $Ge_nO_m^-$ cluster ions. In comparison, the signals measured for bare Ge_n^- cluster ions are practically negligible, and the small signal detected for Ge^- ions is by about a factor 16 below that measured for Ge^+. The GeO-type signals, on the other hand, are comparable for both ion polarities, and the negative ion spectrum exhibits pronounced signals for GeO_2 and GeO_3, which are not observed in the positive spectrum. A similar trend is seen for the clusters with $n = 2.4$, while for $n \geq 5$ only the bare Ge_n^+ clusters are observed.

The spectra measured under SHI irradiation (left panel in Fig. 1) look significantly different from those observed under keV impact. The SNMS spectrum is dominated by the signals measured for Ge atoms and GeO/GeOH molecules, with the hydroxide signal being even larger than that of Ge. We note that the data obtained under SHI and Ar^+ irradiation were measured with different projectile currents, so that the keV-spectra displayed in Fig. 1 need to be divided by approximately a factor 75 in order to facilitate a quantitative comparison of the detected signals. With that correction, the Ge^0 signal measured under SHI impact

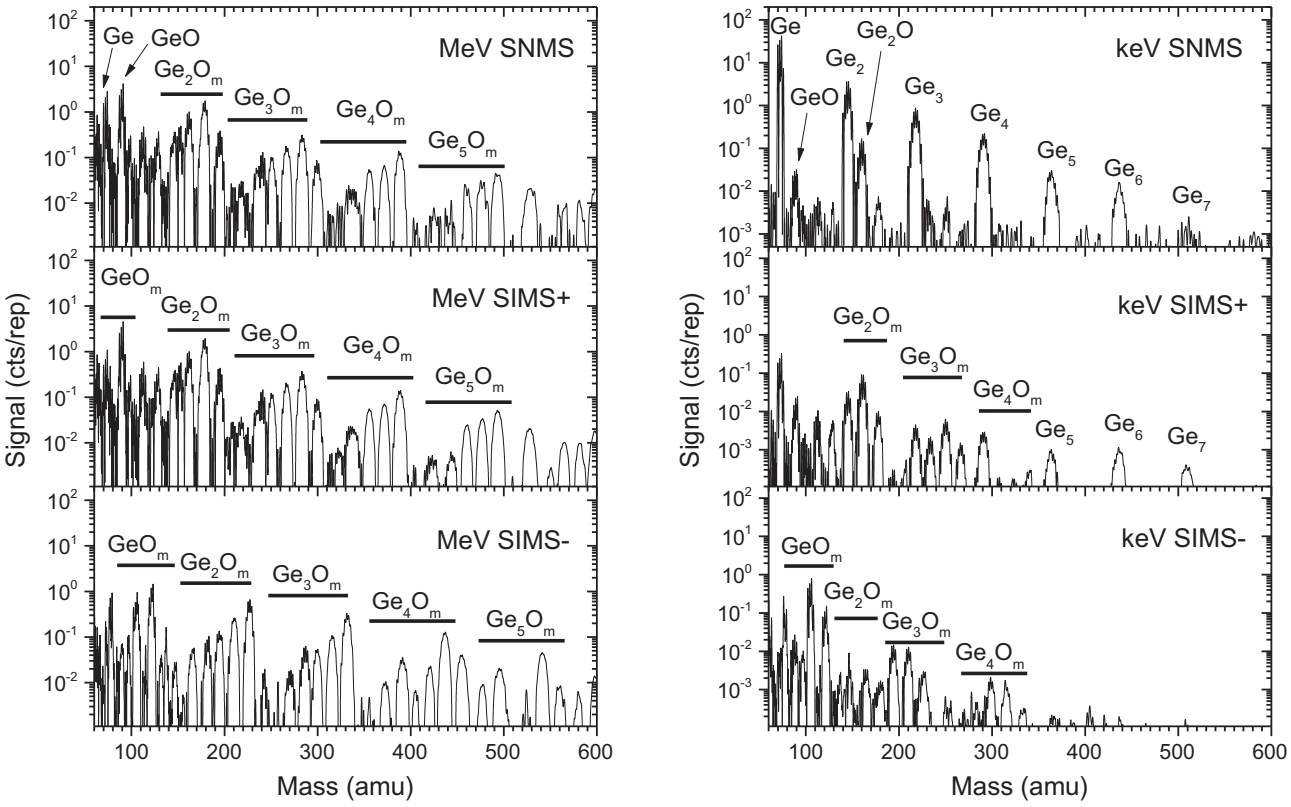

Fig. 1. Mass spectra of post-ionized neutrals and secondary ions measured under irradiation of a dynamically sputter cleaned germanium sample with 4.8 MeV/u $^{197}Au^{26+}$ ions and 5 keV Ar^+ ions at pulse particle currents of 1 nA and 75 nA, respectively. The sample was continuously bombarded with the dc Ar^+ ion beam during the time intervals between different data acquisition gates as described in the text.

is about a factor 5 larger than that detected under keV bombardment. As discussed in detail elsewhere [55], this finding does not necessarily imply a larger sputter yield under SHI impact, since the measured signal represents the *number density* of sputtered particles above the surface rather than their *flux*. Therefore, if the emission velocity distributions of particles sputtered under SHI bombardment were substantially different from those sputtered under keV ion impact, the measured signal ratio would not reflect the sputter yield ratio. Regarding the remaining signals in the spectrum, it should be noted that the SNMS spectrum obtained with the post-ionization laser always contains the positive secondary ion background as well. For instance, comparison with the respective SIMS spectrum reveals that most of the GeO-type signal detected in the SNMS mode is actually due to secondary $[GeOH]^+$ ions. As expected, there is a prominent Ge^0 signal, which is about 4 times that of the corresponding Ge^+ ions. As will be shown below, this signal underestimates the true contribution of sputtered neutral Ge atoms, since the post-ionization efficiency of these species is only about 1%. If corrected for that value, the spectrum shows that the flux of sputtered particles emitted under both irradiation conditions is clearly dominated by neutral Ge atoms. These findings are consistent with the observation of L'Hoir et al. [1], who investigated the secondary ion emission from a germanium crystal surface under impact of 5.6 MeV/u Pb^{28+} ions and found no evidence of Ge ion emission, and emphasize the necessity to look at the sputtered neutrals. As for the keV impact induced spectra, we find a series of Ge_nO_m clusters which, however, here look identical in both SNMS and positive SIMS spectra, revealing that these species are almost exclusively detected as secondary $[Ge_nO_mH_x]^+$ ions. In addition, there is a series of $[Ge_nO_m]K^+$ peaks, which overlay the Ge_nO_m cluster signals and arise from a small potassium contamination of the sample. In fact, the formation of such alkali adduct ions is a common observation in molecular SIMS, since the alkali atoms exhibit a very high positive ionization probability.

3.2. Post-ionization efficiency

A crucial point regarding the quantitative comparison of secondary ion and neutral signals is the post-ionization efficiency, which is determined by the overlap between the laser beam profile, the number density distribution of sputtered neutral particles above the surface and the sensitive volume of the mass spectrometer. Formally, the post-ionization probability can be described by

$$\alpha_X^0 = \int_V n_X(\vec{r}) \cdot p_i(\vec{r}) \cdot T(\vec{r}) d^3r \tag{4}$$

Here, $n_X(\vec{r})$ denotes the number density of neutral particles, $T(\vec{r})$ is the transmission and detection probability for a photo-ion created at position $\vec{r}$ and the integral has to be taken over the sensitive volume. The photoionization probability p_i depends on the laser intensity and will therefore be position dependent according to the laser beam profile. For the single photon ionization process used here, it is expected to depend on the laser intensity I_L as

$$p_i(I_L) = c\,[1-\exp(-I_L/I_{sat})] \tag{5}$$

where I_{sat} is a saturation intensity which depends on the photoabsorption cross section. The proportionality constant in Eq. (5) is unity for single atoms and reflects the branching ratio between laser induced ionization and fragmentation for the case of a sputtered molecule. As long as $I_L \ll I_{sat}$, Eq. (5) describes a linear dependence and the overall post-ionization probability described by Eq. (4) will depend linearly on I_L regardless of the laser beam profile. As soon as I_L reaches I_{sat} anywhere in the sensitive volume, deviations from the linear dependence will occur, until the signal eventually reaches a plateau in the limit of large laser intensities. Unfortunately, the exact shape of the saturation curve is complicated by the fact that both the target density n_X and the detection probability T generally depend on the position within the sensitive volume. Only in the case where the laser beam is defocused

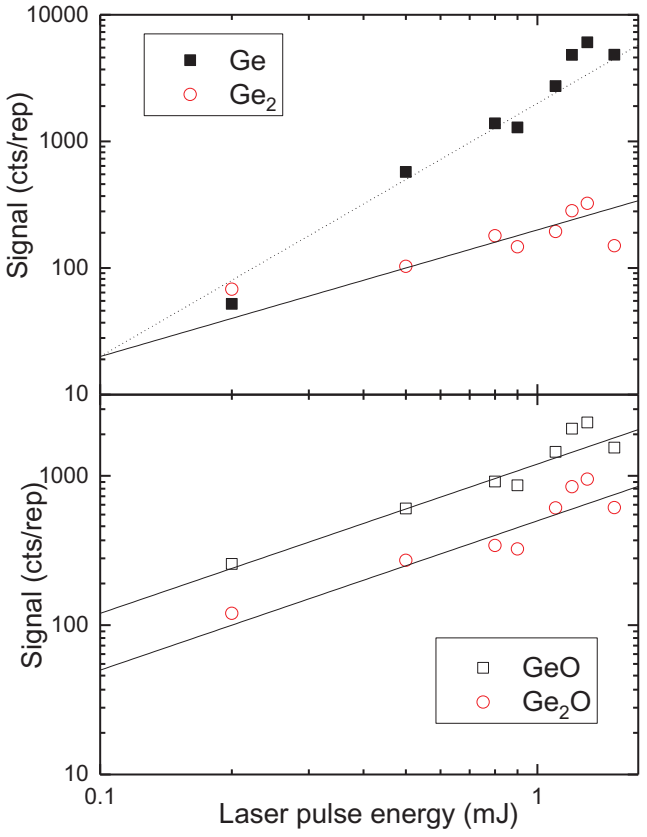

Fig. 2. Laser intensity dependence of a) Ge atoms and Ge_2 dimers, b) Ge_nO_m clusters sputtered from an amorphized Ge surface under irradiation with 4.8 MeV/u $197Au^{26+}$ ions. The surface was sputter cleaned prior to the analysis by dc bombardment with 5 keV Ar^+ ions. The solid lines represent a linear dependence, while the dotted lines represent a dependence according to I_L^2.

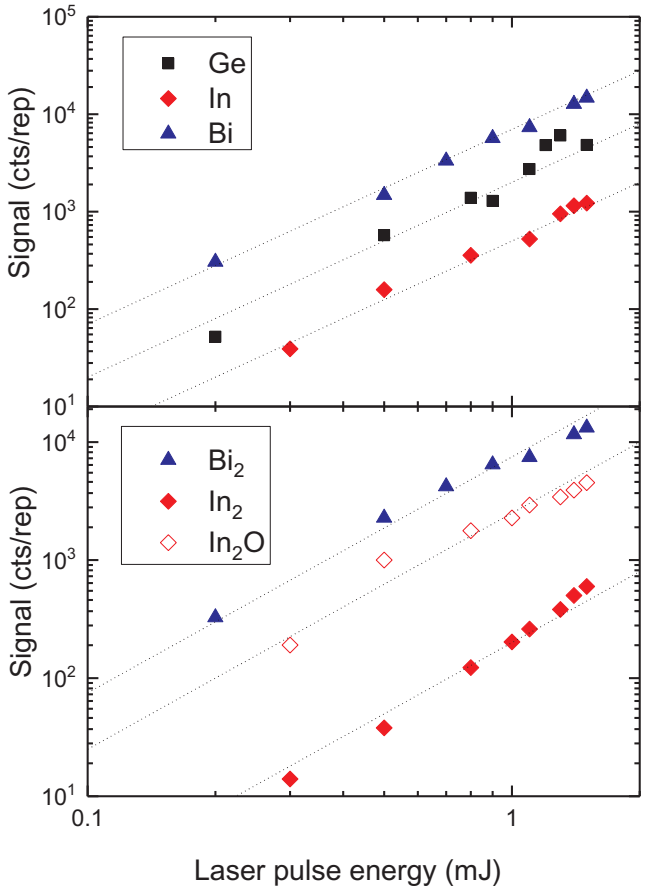

Fig. 3. Laser intensity dependence of In and Bi atoms, In_2 and Bi_2 dimers and In_2O clusters sputtered from the respective metal surface under irradiation with 4.8 MeV/u $197Au^{26+}$ ions. The surface was sputter cleaned prior to the analysis by dc bombardment with 5 keV Ar^+ ions. The dotted lines represent a dependence according to I_L^2.

such as to illuminate the entire sensitive volume with essentially the same intensity, the photoionization probability can be extracted from the integral in Eq. (4) and the laser intensity dependence of the measured post-ionization signal follows the prediction of Eq. (5). While we have measured saturation curves under these conditions in our laboratory, the installation of a VUV laser which is powerful enough to ensure saturation ionization over a large enough volume is not possible at the GSI beamline. Therefore, the laser beam was more tightly focused in the experiments reported here, leading to saturation curves that do not exactly follow the prediction of Eq. (5). Examples for such curves measured for atoms and molecules sputtered under SHI irradiation are shown in Fig. 2, where the post-ionization signal measured under irradiation with 4.8 MeV/u $^{197}Au^{26+}$ ions is plotted against the laser pulse energy measured by the internal intensity monitor of the laser.

Two observations are immediately evident. First, it is seen that the photoionization process of all particles shows no indication of saturation. The plots are made in a double-log fashion, where the linear dependence predicted by Eq. (5) should manifest as a straight line with slope 1. It is seen that straight lines with this slope (solid lines in Fig. 2) can indeed be fitted to the curves measured for Ge_2 as well as GeO and Ge_2O. The apparent scatter of the data points is the same for all signals and must therefore be due to fluctuations in the UNILAC pulse current. For Ge atoms, on the other hand, we observe a steeper increase, corresponding to a slope of about 2 (dotted line in Fig. 2). This findings are quite surprising, since the ionization potential of Ge atoms (7.88 eV) is below the photon energy used here, so that single photon ionization of these atoms should be possible and was indeed previously observed [36]. The published value of the GeO ionization potential (11.1 eV [56]), on the other hand, makes single photon ionization of these molecules from their electronic ground state impossible. The same argument excludes dissociative ionization of larger clusters like Ge_2O_2 as the source of the detected GeO^+ ions. Practically the only possibility for a GeO^+ signal arising from single photon absorption at 157 nm is a neutral GeO^* precursor molecule which is emitted in a metastable (electronically or vibrationally) excited state, thereby lowering its effective ionization potential. Effects of this kind have indeed been observed for some sputtered clusters [57,58]. Alternatively, it is possible that the detected signal is generated by a resonance enhanced two photon ionization process, where the first (excitation) step is saturated, leading to an apparent single photon absorption characteristic.

The question remains why the Ge atom signal does not follow the linear dependence predicted for a single photon absorption process. Inspection of similar curves measured for In and Bi atoms sputtered from the respective metal surfaces as shown in Fig. 3 reveals the same slope as observed for Ge atom. If the laser beam profile remains unchanged upon changing the laser intensity, the linear relation predicted by Eq. (5) must hold for the measured signal as well, since the integral in Eq. (4) becomes proportional to the total laser pulse energy at low laser intensities. As far as the photoionization process is concerned, a deviation from Eq. (5) is possible if either the detected signal originates from (possibly resonance enhanced) dissociative ionization of larger molecular entities such as, for instance, sputtered clusters. In fact, this is a common observation if non-resonant *multiphoton* ionization is used to detect the sputtered neutral species. Under these conditions, it was demonstrated [59] that the apparent photon order of the ionization process (i.e., the slope in plots like Fig. 2) can be modified at low laser

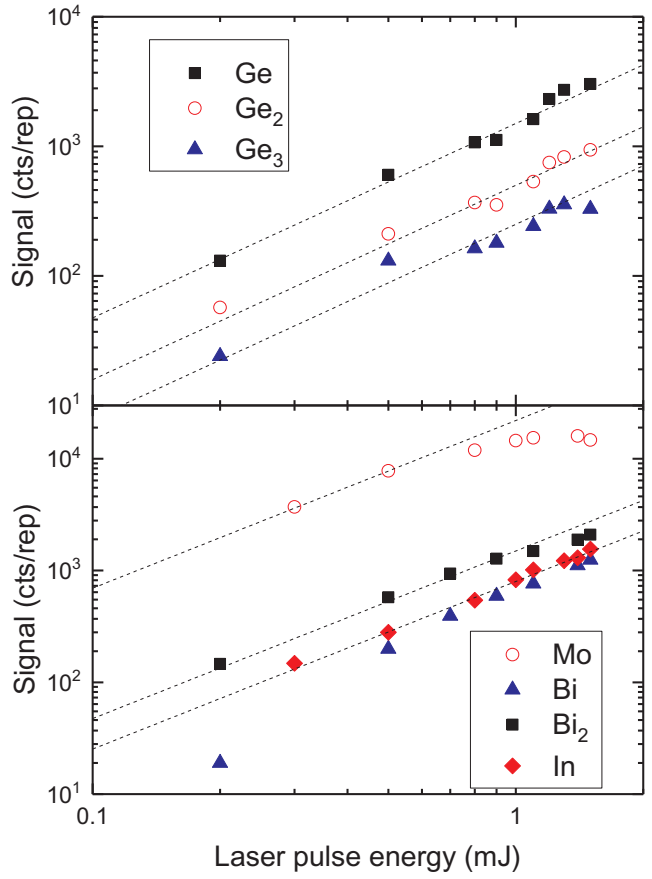

Fig. 4. Laser intensity dependence of a) Ge atoms and Ge_n clusters and b) Mo, Bi and Bi_2 sputtered from the respective solid material under irradiation with 5 keV Ar^+ ions. The solid lines represent a dependence according to $I_L^{1.5}$.

intensities due to signal contributions arising from sputtered clusters.

In order to examine this point further, we look at the signals which were generated *in-situ* under keV ion impact onto the same surface. The resulting laser intensity dependence measured for Ge atoms and clusters is shown in Fig. 4. For comparison, similar curves obtained with the same setup for Mo, Bi and Bi_2 particles have been included. Again, deviations from the predicted linear dependence are found, although the ionization potentials of Mo (7.18 eV), Bi (7.35 eV) and Bi_2 (7.34 eV [60]) are all clearly below the photon energy used here.

It is seen that all curves look very similar and, in particular, exhibit approximately the same slope of 1.5 (indicated by the dashed lines in Fig. 4). We have included the curve measured for molybdenum here, since it is known that Mo atoms exhibit an extraordinarily high SPI cross section at 157 nm [27], and the photoionization of Mo should therefore be saturable at the laser intensities achievable here. Consequently, the corresponding curve shows a clear saturation plateau with a constant signal at laser pulse energies above 1 mJ, which agrees with previously measured ionization efficiency data for Mo [27]. Also in this case, however, the plot indicates a slope of about 1.5 at low laser intensities. The saturation intensity measured previously for Ge is about a factor 40 higher than that of Mo [27,36], thereby suggesting that the post-ionization efficiency for Ge atoms which is reachable here should be of the order of only a few percent. This issue will be further discussed below.

Comparing the keV data measured here with those obtained previously using a more powerful 157 nm laser, one finds a significant difference. While the saturation curves published in Ref. [27] exhibit a strictly linear dependence on the laser intensity over four orders of magnitude, the curves measured here all show a steeper increase at low laser intensity as noted above. Since both data sets were acquired with practically the same ToF spectrometer under the same bombarding conditions (5 keV Ar^+ ions impinging under 45° with respect to the surface normal), the laser intensity dependence measured here must be influenced by changes in the laser beam profile as a function of the set laser intensity. This is in principle possible, since the intensity was varied by changing the discharge voltage of the laser, which may result in modifications of the discharge geometry. Apparently, the beam profile modifications influence the signals measured under keV and SHI bombardment in a different way, leading to different apparent slopes in both experiments. This finding indicates differences in the number density profile $n(\vec{r})$ entering Eq. (4), which may be caused by differences between the emission angle and velocity distributions of the sputtered neutral particles. This point needs to be clarified in future experiments where those distributions are measured, which are, however, outside the scope of the present paper.

From the above discussion, we assume the dependencies measured for all sputtered atoms shown in Figs. 2–4 to reflect the expected single photon ionization behavior. Then, the question arises why the laser intensity dependence of germanium (oxide) clusters sputtered under SHI irradiation appears to be flatter. It is of note that this effect is *not* observed for metal dimers like In_2 or Bi_2 or metal oxide clusters like In_2O, as seen in Fig. 3. A close inspection of the isotope distribution reveals that the signal labeled "Ge_2" in Fig. 2 contains other, not well resolved signals as well. In the same way, the signal labeled "GeO" is found to contain two clearly resolved contributions from GeO and GeOH molecules. Unraveling the two, one finds that the true GeO dependence resembles that of the Ge atoms, while the GeOH signal follows the linear intensity dependence indicated by the solid lines. For Ge_2O, on the other hand, no contribution from Ge_2OH is found. At present, it remains an open question what produces those signals and why their laser intensity dependence appears to be weak.

3.3. Ionization probability

Due to the inherent difficulty to assess the exact value of the post-ionization efficiency α_X^0, the evaluation of absolute ionization probability values from the direct comparison of measured secondary ion and neutral signals via Eq. (1) is difficult. In principle, one combines Eqs. (1) and (2) to obtain

$$\alpha_X^{+,-} = \frac{S(X^{+,-})}{\frac{1}{\alpha_X^0}S(X^0) + S(X^+) + S(X^-)} \tag{6}$$

In order to eliminate the post-ionization efficiency, we again utilize the comparison of data generated under SHI impact with those measured in-situ under 5 keV Ar^+ bombardment. This way, relative values $[\alpha_x^{+,-}]^{MeV}/[\alpha_x^{+,-}]^{keV}$ are determined at the accelerator beam line, which can then be quantified by measurements of $[\alpha_x^{+,-}]^{keV}$ performed in our laboratory at home. For a dynamically sputter cleaned germanium surface bombarded by 5 keV Ar^+ ion, previously measured data of this kind already exist [36]. Using the same protocol here, we find the integrated secondary ion and post-ionized neutral signals listed in Table 1. All signals were normalized to the projectile impact rate and correspond to a singly charged primary ion current of 1 nA.

Comparing the resulting SIMS/SNMS signal ratio obtained for Ar^+ bombardment with that measured previously [36], we can extract the post-ionization efficiency for sputtered Ge atoms and Ge_n clusters up to $n = 4$. It is seen that the post-ionization efficiency obtained here increases with increasing cluster size from ~1% for Ge to ~9%, ~13% and ~19% for Ge_2, Ge_3 and Ge_4, respectively. This finding reflects the general observation that the photoionization cross section increases with increasing cluster size [61]. In fact, the $\alpha_{Ge_n}^0$ values found here almost exactly follow the SPI cross sections determined from the saturation behavior of the SPI process [36]. In principle, we can now use these values to determine the ionization probability for Ge atoms and Ge_n clusters sputtered under SHI irradiation. For Ge atoms, we find a

Table 1
Integrated signals of neutral Ge atoms, Ge_n and Ge_nO_m clusters emitted from a dynamically sputter cleaned germanium surface under irradiation with 4.8 MeV/u $197Au^{26+}$ and 5 keV Ar^+ ions, respectively. The data were normalized to the respective projectile current of 1.1 nA (SHI) and 75 nA (Ar^+). and are given in accumulated cts/rep per nA. The quantity α^+ depicted in the rightmost column of each section denotes the ionization probability of sputtered particles as defined by Eqs. (1) and (6) in the text, where the data displayed for 5 keV Ar^+ projectiles were taken from Ref. [36] and used as a reference in order to calculate the values displayed for 4.8 MeV/u Au^{26+}.

	4.8 MeV/u Au^{26+}				5 keV Ar^+			
	SN	SI +	SI −	α^+	SN	SIMS +	SIMS −	α^+
Ge	397	220	–	3.6E − 03	135	1.2267	–	9.00E − 05
GeO	53	1017	–		0.08	0.13	–	
GeO_2	–	–	375		–	–	2.9	
GeO_3	–	–	484		–	–	0.63	
Ge_2	9	215	–	8.5E − 02	18.7	0.21	–	1.00E − 03
Ge_2O	39	429	28		0.33	0.53	0.03	
Ge_2O_2	–	906	35		–	0.05	0.03	
Ge_2O_3	–	150	81		–	–	0.11	
Ge_2O_4	–	–	176		–	–	0.09	
Ge_2O_5	–	–	322		–	–	0.04	
Ge_3	4	5	–	7.2E − 02	6.1	0.09	–	2.00E − 03
Ge_3O	6	103	–		0.04	0.11	–	
Ge_3O_2	2	98	–		0.17	–	–	
Ge_3O_3	–	115	–		–	–	–	
Ge_3O_4	–	179	45		–	–	–	
Ge_3O_5	–	43	45		–	–	–	
Ge_3O_6	–	–	68		–	–	–	
Ge_3O_7	–	–	181		–	–	–	
Ge_4	–	–	–		1.4	0.03	–	3.50E − 03
Ge_4O_3	2	17	–		–	–	–	
Ge_4O_4	2	28	–		–	–	–	
Ge_4O_5	1	36	5		–	–	–	
Ge_4O_6	5	75	19		–	–	–	
Ge_4O_7	–	–	2		–	–	–	
Ge_4O_8	–	–	10		–	–	–	
Ge_4O_9	–	–	70		–	–	–	

value of $\alpha^+ = 3 \times 10^{-3}$, which is more than an order of magnitude higher than that found under keV bombardment. As seen in Table 1, a similarly enhanced ionization probability is also found for Ge_2 and Ge_3 clusters. Due to the unresolved signal contributions in the spectra measured for these species, the post-ionization signal determined here must be regarded as an upper limit of the true SNMS signal, rendering the α^+-values listed in Table 1 lower limits to the true ionization probability. For Ge_4, the signal is masked by Ge_3O_m signals and therefore not detectable under SHI irradiation. The same holds for the negative secondary ion signals of Ge atoms and all Ge_n clusters, so that the corresponding values of α^- cannot be calculated here, but in any case they must be small compared to the respective α^+.

These findings clearly indicate that the ionization mechanism under electronic sputtering conditions must be different from that occurring in a keV impact induced collision cascade. In that respect, it should be emphasized that the ionization of a sputtered particle ultimately requires electronic excitation. Under nuclear sputtering conditions, the energy transfer between the projectile and the solid proceeds in form of (mostly elastic) atomic collisions, thereby primarily generating fast lattice dynamics in form of a collision cascade, which will then couple energy into the electronic sub-system via inelastic collisions and electronic stopping of all moving particles. The excitation generated this way will be rapidly spread within the solid, so that only that part which remains localized in the cascade volume for a long enough time period until sputter emission occurs (typically a few hundred femtoseconds up to about a picosecond) can contribute to the ionization of sputtered atoms [62]. Under electronic sputtering conditions as investigated here, on the other hand, the primary energy transfer occurs via electronic stopping of the projectile. In that scenario, sputtering occurs as a consequence of energy transfer from the heated electronic sub-system to the cold lattice via electron-phonon coupling. A common approach to describe the resulting energy dynamics is the two temperature model, where the electronic sub-system is treated as a hot electron gas with temperature T_e, which is heated by the electronic energy loss of the projectile. The energy dynamics of the system are then described in terms of two coupled heat conduction equations for the electron and lattice temperatures, respectively. In this scenario, sputtering occurs when the solid material is heated above its critical temperature.

An important feature of the two temperature electronic sputtering model is that – due to the fact that the primarily heated system is the *electronic* system – the electron temperature never falls below the lattice temperature. As a consequence, whenever the lattice temperature is high enough to facilitate the emission of particles, it is at least as high in the electronic sub-system. In other words, sputtered particles always originate from surface regions which are still electronically excited. With that reasoning, it is easy to imagine that the ionization probability of a sputtered particle can be higher than under nuclear sputtering conditions, where most of the transient electronic excitation generated by the projectile impact has already dissipated into the bulk of the solid by the time sputtered particles start leaving the surface [62].

For germanium oxide molecules, a definitive statement regarding the ionization probability is difficult. The reason is that these clusters are practically not detected as post-ionized neutrals under either MeV or keV bombardment of a dynamically sputter cleaned surface, making a quantitative determination of their ionization probability impossible. Since at least the ionization probability measured in keV sputtering experiments depends critically on the oxidation state of the surface, it is not possible to enhance the respective signals via oxidation of the surface without changing α^+. Under SHI irradiation, one finds a positive SIMS/SNMS signal ratio > 0.9 for all detected Ge_nO_m clusters. It is clear, however, that these values must overestimate the ionization probability, since the photoionization of these species is likely not saturated (as seen for GeO and GeO_2 in Fig. 2). In any case, it appears that the germanium oxide clusters produced by electronic sputtering feature much higher ionization probabilities than the bare germanium clusters and are predominantly emitted as positive or negative secondary ions. Comparing the positive and negative secondary ion spectra, one finds different sequences of Ge_nO_m cluster signals, with the *m*-distribution for a specific value of *n* peaking at higher values for negative ions. While the negative SIMS spectrum exhibits maximum intensities at $[GeO_3]^-$, $[Ge_2O_5]^-$, $[Ge_3O_7]^-$, $[Ge_4O_9]^-$ and $[Ge_5O_{11}]^-$, respectively, maximum signal is observed for $[GeO]^+$, $[Ge_2O_2]^+$, $[Ge_3O_4]^+$ $[Ge_4O_6]^+$ and $[Ge_5O_8]^+$ in the positive spectrum. Obviously, the branching between positive and negative ion polarity depends on the composition of the sputtered cluster. Similar results have been found for $[Me_nO_m]^{+,-}$ clusters measured under keV sputtering conditions for different metals Me and were interpreted in terms of a "lattice valence" of the Me atoms in their solid environment [50,63]. In this model, maximum positive or negative secondary ion intensity should be observed for $[Me_nO_{(v+1)n/2}]^-$ and $[Me_nO_{(v-1)n/2}]^+$ clusters, respectively, and neutral clusters would be predicted to center around $[Me_nO_{v\cdot n/2}]^0$. Empirically, one finds the lattice valence *v* from the values m_{max} observed for positive and negative ions via

$$v = \frac{m^+_{max} + m^-_{max}}{n} \tag{7}$$

With the values tabulated in Table 2, one finds $v \sim 1.9$, indicating that the clusters emitted under SHI impact originate from a germanium oxide matrix with approximate GeO stoichiometry. In principle, this finding is surprising, since the keV spectra taken from the same, dynamically sputter cleaned surface exhibit much less oxidic contributions. A possible interpretation of this finding would be that the signals detected under SHI irradiation originate from residual oxide patches at or beneath the surface, which exhibit a high electronic sputter yield and contribute much stronger to the measured spectra than the pure

Table 2
Optimum values m_{max} for secondary $[Ge_nO_m]^{+,-}$ cluster ions emitted from a dynamically sputter cleaned germanium surface under irradiation with 4.8 MeV/u $197Au^{26+}$ ions for different Ge nuclearity n. The value ν depicted in the last column is the lattice valence calculated from these data according to Eq. (7).

n	m^{+}_{max}	m^{-}_{max}	ν
1	1	3	2.0
2	2	5	1.75
3	4	7	1.83
4	6	9	1.87
5	8	11	1.90

germanium crystal. This would also explain the relatively large apparent electronic sputter yield, which appears to be surprising for a pure germanium solid, since this material is known to be quite inert to SHI induced radiation damage even if amorphized [64]. The detection of a sizeable signal of post-ionized neutral GeO molecules would be in line with such an interpretation.

4. Conclusions

The experiments performed here show that the material sputtered from a dynamically cleaned germanium surface under irradiation with swift heavy ions is predominantly composed of neutral Ge atoms. Comparing the signal levels measured for 4.8 MeV/u Au^{26+} ions with those obtained in-situ under 5 keV Ar^{+} irradiation of the same surface, one finds an apparent sputter yield ratio of about 5 between SHI and keV ion bombardment. However, one needs to be careful to interpret the measured SNMS signal ratio in terms of sputter yields, since the emission velocity and angle distributions of neutral atoms ejected under electronic and nuclear sputtering conditions may differ. The ionization probability of the sputtered Ge atoms is found to be < 1%, indicating that the overwhelming majority of the sputtered material is ejected in the neutral state. The probability for a sputtered Ge atom or Ge_n cluster to be emitted as a positive secondary ion is, however, by more than an order of magnitude larger than that for the same particles sputtered under keV impact, while the negative secondary ion signals of these species are negligibly small.

Besides bare germanium atoms and clusters, one finds prominent signals of Ge_nO_m oxide clusters emitted under SHI irradiation, which are much smaller or even negligible under nuclear sputtering conditions. These oxide clusters are almost exclusively detected as positive or negative secondary ions, indicating a relatively high ionization probability of these species. The branching between positive and negative charge state depends on the cluster composition, with the optimum number m of O atoms delivering the largest signal for a given Ge nuclearity n being larger for negative than for positive ions. Using a published secondary ion formation model, these values can be related to the composition of the emitting matrix at the surface [63]. The results indicate that the material ejected under electronic sputtering conditions may originate from an oxidic matrix with approximate GeO stoichiometry. We interpret these findings such that the SHI bombardment must predominantly lead to electronic sputtering of small native oxide grains or patches remaining even at (or below) a dynamically sputter cleaned surface. A further evaluation of this question would require the use of alternative concepts to generate a practically oxygen-free germanium crystal. Corresponding efforts are currently under way and will be implemented during future beam time experiments.

Acknowledgement

The authors are greatly indebted to W. Saure and A. Siegmund for technical assistance during the setup of the experiment. We also acknowledge financial support from the German Ministry of Science (BMBF) in the framework of the Verbundprojekt 05K13PG1 and 05K16PG1 “Ion Induced Materials Characterization and Modification”.

References

[1] A. L'Hoir, C. Koumeir, S. Della Negra, P. Boduch, P. Roussel-Chomaz, A. Cassimi, M. Chevallier, C. Cohen, D. Dauvergne, M. Fallavier, D. Jacquet, B. Manil, J.C. Poizat, C. Ray, H. Rothard, D. Schmaus, M. Toulemonde, Study of ion emission from a germanium crystal surface under impact of fast Pb ions in channeling conditions, Nucl. Instrum. Methods B 267 (2009) 876–880.
[2] H. Hijazi, H. Rothard, P. Boduch, I. Alzaher, F. Ropars, A. Cassimi, J.M. Ramillon, T. Been, B.B. d'Etat, H. Lebius, L.S. Farenzena, E.F. da Silveira, Interaction of swift ion beams with surfaces: sputtering of secondary ions from LiF studied by XY-TOF-SIMS, Nucl. Instrum. Methods B 269 (2011) 1003–1006.
[3] H. Hijazi, L.S. Farenzena, H. Rothard, P. Boduch, P.L. Grande, E.F. da Silveira, Cluster ion emission from LiF induced by MeV Nq+ projectiles and 252Cf fission fragments, Eur. Phys. J. D 63 (2011) 391–400.
[4] H. Hijazi, H. Rothard, P. Boduch, I. Alzaher, A. Cassimi, F. Ropars, T. Been, J.M. Ramillon, H. Lebius, B. Ban-d'Etat, L.S. Farenzena, E.F. da Silveira, Electronic sputtering: angular distributions of (LiF)nLi+ clusters emitted in collisions of Kr (10.1 MeV/u) with LiF single crystals, Eur. Phys. J. D 66 (2012) 68.
[5] H. Hijazi, T. Langlinay, H. Rothard, P. Boduch, F. Ropars, A. Cassimi, L.S. Farenzena, E.F. da Silveira, Strong perturbation effects in heavy ion induced electronic sputtering of lithium fluoride, Eur. Phys. J. D 68 (2014) 185.
[6] R. Martinez, L. Th, P. Boduch, A. Cassimi, H. Hijazi, F. Ropars, P. Salou, E.F.d. Silveira, H. Rothard, Electronic sputtering of thin lithium fluoride films induced by swift heavy ions, Mater. Res. Express 2 (2015) 076403.
[7] W. Assmann, B. Ban-d'Etat, M. Bender, P. Boduch, P.L. Grande, H. Lebius, D. Lelievre, G.G. Marmitt, H. Rothard, T. Seidl, D. Severin, K.O. Voss, M. Toulemonde, C. Trautmann, Charge-state related effects in sputtering of LiF by swift heavy ions, Nucl. Instrum. Methods B 392 (2017) 94–101.
[8] M.G. Blain, E.A. Schweikert, E.F. Da Silveira, Clusters as projectiles for SIMS, J. Phys-Paris 50 (1989) C2–85.
[9] C.C. de Castro, I.S. Bitensky, E.F. da Silveira, Desorption of H− ions from solid surfaces induced by MeV ion impact, Nucl. Instrum. Methods B 132 (1997) 561–570.
[10] J.A.M. Pereira, E.F. Da Silveira, K. Wien, MeV nitrogen bombardment of LiF: from the nuclear to the electronic sputtering regimes, Radiat. Eff. Defects Solids 142 (1997) 247–255.
[11] E.F. Da Silveira, S.B. Duarte, E.A. Schweikert, Multiplicity analysis: a study of secondary particle distribution and correlation, Surf. Sci. 408 (1998) 28–42.
[12] J.A.M. Pereira, E.F. Da Silveira, Li/sup +/ secondary ion energy distributions probed by fast N/sub 2//sup +/ and N/sup q+/ bombardment of LiF, Nucl. Instrum. Methods B 146 (1998) 185–189.
[13] J.A.M. Pereira, I.S. Bitensky, E.F. da Silveira, Effects of charge state and number of constituents of MeV projectiles on secondary ion emission yields from LiF, Nucl. Instrum. Methods B 135 (1998) 244–249.
[14] C.C. de Castro, I.S. Bitensky, E.F. da Silveira, M. Most, K. Wien, Energy distribution of H+ ions desorbed from metal surfaces by MeV ion impact, Int. J. Mass Spectrom. 173 (1998) 1–15.
[15] J.A.M. Pereira, E.F. da Silveira, Li+ secondary ion energy distributions probed by fast N2+ and Nq+ bombardment of LiF, Nucl. Instrum. Methods B 146 (1998) 185–189.
[16] J.A.M. Pereira, I.S. Bitensky, E.F. da Silveira, Nonlinear effects in ion emission from LiF induced by N+ and N-2(+) MeV ion impact, Int. J. Mass Spectrom. 174 (1998) 179–191.
[17] J.A.M. Pereira, E.F. da Silveira, Combined TOF-MS/RBS analysis of LiF thin films bombarded by MeV nitrogen ions, Nucl. Instrum. Methods B 136 (1998) 779–783.
[18] J.A.M. Pereira, E.F. da Silveira, Li+ secondary ion energy distributions probed by fast N-2(+) and Nq+ bombardment of LiF (vol 146, pg 185, 1998), Nucl. Instrum. Methods B 155 (1999) 206.
[19] J.A.M. Pereira, E.F. da Silveira, Cluster and velocity effects on yields and kinetic energy distributions of Li+ desorbed from LiF, Phys. Rev. Lett. 84 (2000) 5904–5907.
[20] T. Jalowy, R. Neugebauer, M. Hattass, J. Fiol, F. Afaneh, J.A.M. Pereira, V. Collado, E.F. da Silveira, H. Schmidt-Bocking, K.O. Groeneveld, Dynamics of secondary ion emission: novel energy and angular spectrometry, Nucl. Instrum. Methods B 193 (2002) 762–767.
[21] T. Jalowy, R. Neugebauer, K.O. Groeneveld, C.R. Ponciano, L.S. Farenzena, E.F. da Silveira, XY-TOF technique for large ion source mass spectrometers, Int. J. Mass Spectrom. 219 (2002) 343–350.
[22] F. Alberto Fernandez-Lima, O.P. Vilela Neto, A. Silva Pimentel, M.A.C. Pacheco, C.R. Ponciano, M.A.C. Nascimento, E.F. da Silveira, Theoretical and experimental study of negative LiF clusters produced by fast ion impact on a polycrystalline 7LiF target, J. Phys. Chem. A 113 (2009) 15031–15040.
[23] F.A. Fernandez-Lima, O.P. VilelaNeto, A.S. Pimentel, C.R. Ponciano, M.A.C. Pacheco, M.A.C. Nascimento, E.F.d. Silveira, A theoretical and experimental study of positive and neutral LiF clusters produced by fast ion impact on a polycrystalline LiF target, J. Phys. Chem. A 113 (2009) 1813–1821.
[24] W. Assmann, M. Toulemonde, C. Trautmann, Electronic sputtering with swift heavy ions, in: R. Behrisch, W. Eckstein (Eds.), Sputtering by Particle Bombardment, Springer, Berlin, 2007, pp. 401–450.
[25] D. Lipinsky, R. Jede, J. Tumpner, O. Ganschow, A. Benninghoven, Electron-beam

impact postionization of sputtered neutrals, Surf. Interf. Anal. 9 (1986) 73-73.
[26] H. Oechsner, E. Stumpe, Sputtered neutral mass spectrometry (SNMS) as a tool for chemical surface analysis and depth profiling, Appl. Phys. 14 (1977) 43–47.
[27] A. Wucher, Laser postionization - fundamentals, in: J.C. Vickerman, D. Briggs (Eds.), TOF-SIMS: Materials analysis by mass spectrometry, IM Publications and SurfaceSpectra, 2013, pp. 217–246.
[28] J.B. Pallix, U. Schuehle, C.H. Becker, L. Huestis, Advantages of single-photon ionization over multiphoton ionization for mass spectrometric surface analysis of bulk organic polymers, Anal. Chem. 61 (1989) 805–811.
[29] N.P. Lockyer, J.C. Vickerman, Single photon ionisation mass spectrometry using laser-generated vacuum ultraviolet photons, Laser Chem. 17 (1997) 139–159.
[30] M. Wahl, A. Wucher, VUV photoionization of sputtered neutral silver clusters, Nucl. Instrum. Methods B 94 (1994) 36–46.
[31] L.K. Takahashi, J. Zhou, K.R. Wilson, S.R. Leone, M. Ahmed, Imaging with mass spectrometry: a secondary ion and VUV-photoionization study of ion-sputtered atoms and clusters from GaAs and Au, J. Phys. Chem. A 113 (2009) 4035–4044.
[32] I.V. Veryovkin, W.F. Calaway, J.F. Moore, M.J. Pellin, J.W. Lewellen, Y.L. Li, S.V. Milton, B.V. King, M. Petravic, A new horizon in secondary neutral mass spectrometry: post-ionization using a VUV free electron laser, Appl. Surf. Sci. 231–2 (2004) 962–966.
[33] L. Hanley, P.D. Edirisinghe, W.F. Calaway, I.V. Veryovkin, M.J. Pellin, J.F. Moore, 7.87 eV postionization of peptides containing tryptophan or derivatized with fluorescein, Appl. Surf. Sci. 252 (2006) 6723–6726.
[34] A. Wucher, W. Berthold, H. Oechsner, The charge state of sputtered metal clusters, in: A. Benninghoven, Y. Nihei, R. Shimizu, H.W. Werner (Eds.), Secondary Ion Mass Spectrometry (SIMS IX), Wiley & Sons, Yokohama, 1993, pp. 100–103.
[35] A. Wucher, R. Heinrich, R.M. Braun, K.F. Willey, N. Winograd, Vacuum ultraviolet single photon versus femtosecond multiphoton ionization of sputtered germanium clusters, Rapid Commun. Mass Spectr. 12 (1998) 1241–1245.
[36] R. Heinrich, A. Wucher, Yields and energy distributions of sputtered semiconductor clusters, Nucl. Instrum. Methods B 140 (1998) 27–38.
[37] R. Heinrich, C. Staudt, M. Wahl, A. Wucher, Ionization probability of sputtered clusters, in: A. Benninghoven, P. Bertrand, H.-N. Migeon, H.W. Werner (Eds.), Secondary Ion Mass Spectrometry (SIMS XII), Elsevier Science, 1999, pp. 111–114.
[38] A. Wucher, R. Heinrich, C. Staudt, A method for quantitative determination of secondary ion formation probabilities, in: A. Benninghoven, P. Bertrand, H.N. Migeon, H.W. Werner (Eds.), Secondary Ion Mass Spectrometry (SIMS XII), Elsevier Science, 1999, pp. 143–146.
[39] C. Staudt, R. Heinrich, A. Wucher, Formation of large clusters during sputtering of silver, Nucl. Instrum. Methods B 164–165 (2000) 677–686.
[40] A. Wucher, Laser post-ionisation: fundamentals, in: J.C. Vickerman, D. Briggs (Eds.), ToF-SIMS: Surface Analysis by Mass Spectrometry, IM Publications and Surface Spectra Limited, Chicester, 2001, pp. 347–373.
[41] C. Staudt, A. Wucher, Generation of large indium clusters by sputtering, Phys. Rev. B 66 (2002) 075419-075411.
[42] S. Meyer, C. Staudt, A. Wucher, Ionization probability of atoms and molecules sputtered from a cesium covered silver surface, Appl. Surf. Sci. 203–204 (2003) 48–51.
[43] A. Samartsev, A. Wucher, Yields and ionization probabilities of sputtered Inn particles under atomic and polyatomic Au_m ion bombardment, Appl. Surf. Sci. 252 (2006) 6474–6477.
[44] P. Mazarov, A. Samartsev, A. Wucher, Determination of energy dependent ionization probabilities of sputtered particles, Appl. Surf. Sci. 252 (2006) 6452–6455.
[45] A. Wucher, H. Oechsner, Absolute ionization probabilities in secondary ion emission from clean metal surfaces, in: J. Romig, W.F. Chambers (Eds.), Proc. of 21st Annual Conference of the Microbeam Analysis Society 1986, San Francisco Press, 1986.
[46] K. Franzreb, A. Wucher, H. Oechsner, Formation of neutral and positively charged clusters during sputtering of silver, Surf. Sci. 279 (1992) L225–L230.
[47] A. Wucher, M. Wahl, Cluster emission in sputtering, in: A. Benninghoven, B. Hagenhoff, H.W. Werner (Eds.), Secondary Ion Mass Spectrometry (SIMS X), Wiley & Sons, 1995, pp. 65–72.
[48] C. Staudt, A. Wucher, Resonance Ionization Spectroscopy, AIP Press, Manchester, 1998, pp. 217–222.
[49] J. München, D. Lipinsky, H.F. Arlinghaus, Signals of secondary ions and resonantly and nonresonantly ionized neutrals sputtered from binary alloys as a function of oxygen exposure, Surf. Interf. Anal. 45 (2013) 117–121.
[50] A. Benninghoven, Developments in secondary ion mass spectroscopy and applications to surface studies, Surf. Sci. 53 (1975) 596–625.
[51] A. Wucher, H. Oechsner, Emission energy dependence of ionization probabilities in secondary ion emission from oxygen covered Ta, Nb and Cu surfaces, Surf. Sci. 199 (1988) 567–578.
[52] F. Meinerzhagen, L. Breuer, H. Bukowska, M. Herder, M. Bender, D. Severin, H. Lebius, M. Schleberger, A. Wucher, SHIPS: a new setup for the investigation of swift heavy ion induced particle emission and surface modifications, Rev. Sci. Instrum. 87 (2016).
[53] L. Breuer, F. Meinerzhagen, M. Bender, D. Severin, A. Wucher, Secondary ion & neutral mass spectrometry using swift heavy ions, Nucl. Instrum. Methods B (in press) (2015).
[54] M. Toulemonde, Irradiation by swift heavy ions: Influence of the non-equilibrium projectile charge state for near surface experiments, Nucl. Instrum. Methods B 250 (2006) 263–268.
[55] L. Breuer, P. Ernst, M. Herder, F. Meinerzhagen, M. Bender, D. Severin, A. Wucher, Mass spectrometric investigation of material sputtered under swift heavy ion bombardment, Nucl. Instrum. Methods B (2017), http://dx.doi.org/10.1016/j.nimb.2017.10.019.
[56] K.P. Huber, G. Herzberg, Molecular Spectra and Molecular Structure. IV. Constants of Diatomic Molecules, Van Nostrand Reinhold Company Inc., New York, 1979.
[57] A. Wucher, Internal energy of sputtered metal clusters, Phys. Rev. B 49 (1994) 2012–2020.
[58] A. Wucher, C. Staudt, S. Neukermans, E. Janssens, F. Vanhoutte, R.E. Silverans, P. Lievens, On the internal energy of sputtered clusters, New. J. Phys. 10 (2008) 1–22.
[59] S. Kaesdorf, M. Hartmann, H. Schroeder, K.L. Kompa, Influence of laser parameters on the detection efficiency of sputtered neutrals mass spectrometry based on non-resonant multiphoton ionization, Int. J. Mass Spectrom. Ion Processes 116 (1992) 219–247.
[60] R.K. Yoo, B. Ruscic, J. Berkowitz, Photoionization mass spectrometric studies of Sb2 and Bi2, J. Chem. Phys. 99 (1993) 8445–8450.
[61] A. Wucher, Formation of clusters in sputtering, Izv. Akad. Nauk. Ser. Fiz. 66 (2002) 499–508.
[62] A. Wucher, B. Weidtmann, A. Duvenbeck, A microscopic view of secondary ion formation, Nucl. Instrum. Methods B 303 (2013) 108–111.
[63] C. Plog, L. Wiedmann, A. Benninghoven, Empirical formula for the calculation of secondary ion yields from oxidized metal surfaces and metal oxides, Surf. Sci. 67 (1977) 565–580.
[64] A. Kamarou, W. Wesch, E. Wendler, A. Undisz, M. Rettenmayr, Radiation damage formation in InP, InSb, GaAs, GaP, Ge, and Si, due to fast ions, Phys. Rev. B 78 (2008).